Available online at www.sciencedirect.com
SCIENCE DIRECT
Journal of the European Ceramic Society 26 (2006) 2219–2230
www.elsevier.com/locate/jeurceramsoc

Titanium effect on phase transformation and sintering behavior of transition alumina

Sylvie Lartigue-Korinek [a,*], Corinne Legros [b], Claude Carry [c], Frédéric Herbst [b]

[a] *Centre d'Etudes de Chimie Métallurgique, CNRS UPR 2801, 15 rue Georges Urbain, 94400 Vitry-sur-Seine, France*
[b] *Laboratoire d'Etude des Matériaux Hors Equilibre, CNRS UMR 8647, Université Paris Sud, 91405 Orsay Cedex, France*
[c] *Laboratoire de Thermodynamique et Physico-Chimie des Matériaux, CNRS-INPG/UJF UMR 5614, BP 75, 38402 Saint-Martin-d'Hères Cedex, France*

Received 17 October 2004; received in revised form 21 March 2005; accepted 9 April 2005
Available online 23 May 2005

Abstract

The sintering behavior of doped γ-alumina powders studied by dilatometry and electron microscopy is analysed with a particular emphasis on the role of titanium on the various densification steps. Compared with other doping elements, such as Mg, Y and Zr, which do not improve α-phase densification, titanium enhances this densification step by a fast decrease of internal colony porosity. This internal densification of single crystalline zones is attributed to the lengthening of the elementary bricks in titanium-doped samples. A transient increase in densification rate is also observed, corresponding to the precipitation when during grain growth, grain boundaries become saturated with titanium. Final densities close to the theoretical values are obtained.

Keywords: Sintering; Al_2O_3; Doping elements; Microstructure; Electron microscopy; TiO_2; γ-Al_2O_3

1. Introduction

In recent years, there has been an increasing interest in the synthesis of nanocrystalline metal oxides. In particular, nanocrystalline aluminas could be of interest for technological applications for their electronic and mechanical properties. Starting from nanostructured powders, dense nanocrystalline ceramics, such as TiO_2, ZrO_2, CeO or Y_2O_3 have been obtained.[1–3]. However, most of these powders are metastable and undergo phase transformations during sintering. This is the case for γ-alumina for which the transformation to the α-phase is unfortunately accompanied by the development of a vermicular microstructure that requires very high sintering temperatures to achieve high final density, thus leading to large grain sizes.[4] Improvement may be obtained by seeding the initial precursors gels or powders with α-Al_2O_3,[5,6] by pressure sintering methods,[7] by doping of γ-powders with different elements[8,9] or by colloidal processing methods.[10–12]

Because our ultimate goal is to prepare α-Al_2O_3 nanoceramics starting from nanocrystalline γ-Al_2O_3, without pressure assisted sintering, we have examined the role of seeding in α-alumina and the role of dopants on the sintering behavior of γ-alumina in relation with the microstructural evolution of the material. First results on undoped γ-alumina[6,13] have shown that after the phase transformation, the microstructure of porous alumina is a mosaic of clusters, called colonies, consisting of nanosized elementary bricks with close crystallographic orientations; these colonies can be considered as porous singlecrystalline zones.[4] They result from coupled mechanisms of transformation-rearrangement-coalescence from nucleation sites.[5,6,13]

The current investigation presents the effect of doping elements, more especially the effect of titanium on sintering behavior of γ-alumina compacts. As is the case for most doping elements in alumina, titanium has a conflicting influence on the sintering of alumina. On the one hand, it has

* Corresponding author. Tel.: +33 156 703031; fax: +33 146 750433.
E-mail address: sylvie.lartigue@cecm.cnrs.fr (S. Lartigue-Korinek).

0955-2219/$ – see front matter © 2005 Elsevier Ltd. All rights reserved.
doi:10.1016/j.jeurceramsoc.2005.04.006

a beneficial role on densification,[14–17] on the other hand, it promotes grain growth and contributes to the development of anisotropic microstructures.[18–20] Doping elements have generally a low solubility limit in α-alumina and segregate to grain boundaries (GBs) or precipitate when the GBs are saturated.[21–24]

γ-Alumina is a metastable phase with an open spinel structure that is known to incorporate a larger amount of various doping elements than α-alumina does.[25,26] Doping procedure should be considered in regards of this incorporation: sol–gel and coprecipitation are better routes than impregnation way.[26] Thus, doping could modify the phase transformation temperature and kinetics and lead to variations in relative density.[9,27]

The dopants influence the GB diffusion properties and GB mobility during grain growth. From creep experiments, it has been deduced that yttrium and zirconium decrease GB diffusion[24,28–32], meanwhile Ti and Mg increase GB diffusion in comparison to undoped alumina.[33] Titanium addition is known to strongly improve densification of α-alumina.[14,17] This increase in densification is interpreted as an increase in intergranular diffusion associated with an increase in GB mobility.[20,34,35] Moreover, the increase in diffusion is related to the increase in aluminium vacancies concentration that has been found to depend on the titanium content through a power law relation.[36] Grain growth in Ti-doped polycrystals may lead to highly anisotropic microstructures which are usually attributed to the presence of a liquid phase containing silicon as main impurity.[20,37–40] It is interesting to note that alumina doped with only titanium or only silicon does not display anisotropic grain growth.[20,37] In Ti-doped alumina anisotropic grain growth occurs at a critical grain size that increases as the dopant level increases.[41] It is suggested to occur when a small population of grains has attained a critical size while the other grains have not grown noticeably; this anisotropy could be related to the possibility for the sample to present a transition between segregation at GBs to precipitation of second phase when a GB saturation level is attained as previously discussed in the case of yttrium doping.[28] As a matter of fact, for a given doping content, normal grain growth is observed if the initial powder grain size is larger than the critical grain size for which precipitation occurs.[41] Referring to GB and volume diffusion transitions, such critical titanium amount has been already reported without explicit grain size considerations.[14]

The present paper is organized in the following manner. Section 2 describes details of material preparation, sintering experiments and microstructural investigations techniques. Section 3 presents the results on titanium influence on macroscopic sintering behavior and on the microstructural evolution during densification. For comparison, some results on the effects of other doping elements (magnesium, yttrium and zirconium) are reported. Results are discussed in terms of dopant spatial distribution in Section 4. Section 5 concludes the paper.

2. Experimental procedure

Ti-doped samples are prepared from the same undoped batch (ND) of Baikalox CR125 commercial grade (Baikowski Chimie, France), an alum derived γ-alumina with a very high specific area (≈100 m^2/g), a median particle size of 0.27 μm and α initial content less than 0.5%. Impurity analysis by the ICP-AES method showed the major impurities were as follows (ppm): Na (9), K (14), Fe (3), Si (9) and Ca (<1).

The incorporation of the doping element in the γ-alumina powder is achieved by the following procedure. Ten grams of the undoped powder is dispersed in about 30 ml of propane-2-ol using a vibrating stirrer to obtain slurry. For a given doping level, the corresponding amount of a titanium isopropoxide solution is poured into the alumina slurry and stirred for 2 min. Thereafter, distilled water is quickly added to hydrolyse the Ti-isopropoxide. The water to alkoxide molar ratio is about 10:1. Then, each slurry is dried and later calcined under oxygen flowing at 800 °C for 24 h in order to eliminate solvent traces, to decompose titanium hydroxides and to yield a homogeneous distribution of the dopant on the surface of the alumina particles.

The expected doping level varies from 300 to 9600 ppm Ti/Al and doped samples are labeled by their cationic ratio Ti/Al (ppm/100), for example 64Ti means a doping level of 6388 ppm Ti/Al (or 9360 ppm wt TiO_2). The same convention is used for the other doping elements; for example 31Y means a doping level of 3150 ppm Y/Al.

The average concentration of Ti and impurities were measured in powder sample by ICP-AES or ICP-OES methods. The Ti concentrations were typically of (ppm), respectively for 16Ti (1740 ± 20), 32Ti (3135 ± 30), 64Ti (6578 ± 62) and 96Ti (10699 ± 100). Concentration of low level of impurities, such as Si was found to be lower than the detection limit. However, our samples are highly doped so the impurity contents are largely lower than the doping levels. Furthermore, most of the results concern initial stages of sintering for which the grain sizes are so small that the large differences in sintering behavior discussed here as a function of the dopant nature cannot be attributed to the presence of impurities. It should be also noted that this doping procedure does not modify the α content of the powder, so all doped powders used in this work can be considered as unseeded powders.

After cold isostatic pressing (CIP) at a pressure of 250 MPa, green compacts for sintering are dry-grinded into cylindrical samples 6 mm in diameter and 100 mm in height. The shrinkage is followed by dilatometry (TMA92 Setaram, France). All sintering treatments are performed in static air and all samples are heated up to 800 °C at 10 °C min^{-1}. They are then heated up to 1450 °C (or 1550 °C) under a constant heating rate of 1 °C or 10 °C min^{-1}, and rapidly cooled. Another thermal treatment, named standard sintering treatment in the following, has been carried out: it corresponds to heating up to 1450 °C with a 20 °C min^{-1} heating rate, followed by annealing 4 h 15 min at 1450 °C. These conditions have

been chosen in order to increase the nucleation site density, enhance the particle rearrangement during the phase transformation and improve the α-phase densification as will be explained in a detailed manner in a forthcoming paper.

Densities and densification rate curves (as function of temperature T or time t) are computed from the recorded shrinkage data and from the final densities measured by using Archimedes's method on cooled samples. Some densification runs have been interrupted at different stages of the heat treatment in order to carry out microstructural analysis by scanning or transmission electron microscopy (STEM or TEM). Conventional TEM experiments are performed on a JEOL 2000EX operating at 200 kV. Thin foils are prepared by mechanical polishing and ion milling at 5 kV and coated with a carbon layer to avoid charging under the electron beam. Microstructures are also observed by Scanning Electron Microscopy (SEM) on fractured surfaces. Grain sizes are estimated by linear intercept method on SEM micrographs, considering that fracture is mostly intergranular.

3. Results and analysis

3.1. Macroscopic sintering behavior of Ti-doped γ-alumina

Fig. 1 compares the densification behavior of a 32Ti-doped alumina sample sintered in constant heating rate conditions (1 °C min^{-1}) with that of an undoped (ND) and magnesium, yttrium, zirconium doped alumina samples prepared (same doping procedure but from nitrate salts instead of alkoxides) with same range of doping level (2500 ppm Mg/Al, 3100 ppm Y/Al and 2500 ppm Zr/Al). The two classical regimes of densification (R1 and R2) of such γ-alumina compacts are observed.[6] R1 is the rapid densification associated with the phase transition of γ-alumina to the stable α-phase in the 1000–1150 °C temperature range and R2 is the slower densification of α-phase at higher temperatures. While yttrium and zirconium doped compacts shift the first densification rate peak R1 to higher temperatures (up to 50 °C increase), titanium and magnesium have a less pronounced effect. The relative density variation $\Delta\rho_R$ during the phase transformation is slightly increased by the presence of Y and Mg; Zr has practically no influence although Ti decreases $\Delta\rho_R$. These observations are in agreement with the dopants influence found on the rate of transformation from γ to α phase.[42]

For the R2 densification regime, Mg, Y and Zr do not improve the densification in α-phase, but Ti increases it significantly. In addition to these two regimes of densification, there are shoulders on the density curve of 32Ti and 31Y samples with corresponding additional densification rate peaks (AP). Such transient increase in densification rate has been already reported for Y-doped alumina.[9]

Fig. 2 illustrates the effect of Ti-doping level on densification under the same constant heating rate conditions (1 °C min^{-1}) up to 1450 °C. Titanium addition has a slight influence on the first densification rate peak R1, the temperature of the R1 peak increases by a few degrees with titanium

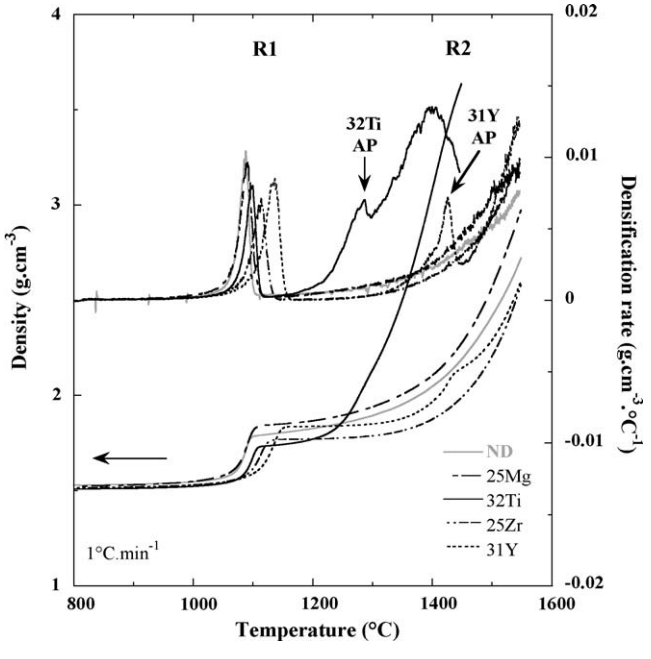

Fig. 1. Comparison of densification curves (densities and densification rates) of titanium doped (3200 ppm Ti/Al) γ-alumina compacts with undoped (ND), magnesium doped (2500 ppm Mg/Al), yttrium doped (3100 ppm Y/Al) and zirconium doped (4500 ppm Zr/Al) γ-alumina compacts (cold isostatic pressing: 250 MPa, heating rate: 1 °C min^{-1} from 850 °C).

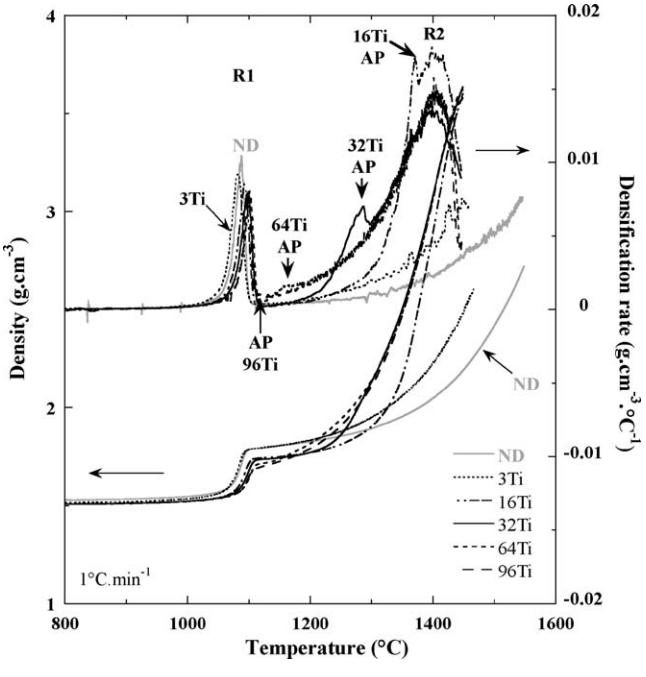

Fig. 2. Densification curves (densities and densification rates) of Ti-doped (300, 1600, 3200, 6400 and 9600 ppm Ti/Al) and undoped (ND) γ-alumina compacts with constant heating rates (1 °C min^{-1} from 800 °C). A high densification occurs for all Ti-doped samples. An additional densification rate peak (AP) is observed for Ti level equal or higher than 1600 ppm.

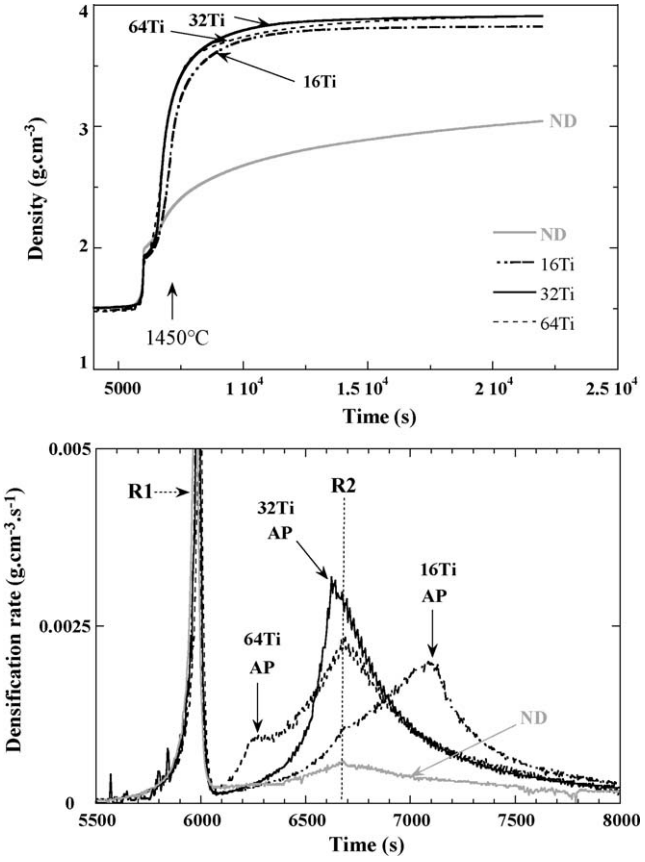

Fig. 3. Densification curves (densities and densification rates) of Ti-doped (1600, 3200, and 6400 ppm Ti/Al) and undoped (ND) γ-alumina compacts heated at 20 °C min^{-1} from 800 °C → 1450 °C + 4 h 15 min at 1450 °C (standard sintering treatment). High densities are attained well before the end of the thermal treatment. The second densification regime R2 occurs always at the same temperature and the additional peak (AP) is displaced towards the beginning of the dwelling step as the doping level increases.

content. The relative density variation $\Delta\rho_R$ decreases as the titanium level increases. On the other hand, Ti-doping increases significantly the R2 densification regime. Moreover, whatever the Ti-doping level, the R2 α-phase densification rate peak occurs at the same temperature. For Ti-doping level higher than 3Ti, final densities are higher than 90% of the theoretical density and an additional densification rate peak (AP) is observed; its temperature decreases with increasing titanium levels, as it will be discussed later on.

Fig. 3 shows the densification behavior (densities and densification rates versus time) of Ti-doped samples for the standard sintering treatment (20 °C min^{-1} up to 1450 °C + 4 h 15 min). The overall characteristics of these curves are similar to those of the previous treatment, however the relative density variation $\Delta\rho_R$ during phase transformation is higher but remains lower than for undoped sample. Densities of Ti-doped aluminas are very high, larger than 95% of theoretical density. In particular, the maximal density of the 32Ti-doped sample is attained for times as short as 2 h at 1450 °C, suggesting that after this time only grain growth takes place. As previously seen, the maximum of the densification rate of the α-phase (R2) occurs at the same time for all samples and the additional densification peak (AP) moves toward the beginning of the annealing at 1450 °C as the doping level increases. It should be noted that densification is the highest for the 32Ti-doped sample (98% of the theoretical one), for which the additional densification rate peak (AP) is concurrent with the maximum densification rate peak R2.

3.2. Microstructural behavior of Ti-doped γ-alumina

3.2.1. Final microstructures

At the end of all the thermal treatments, microstructures of the Ti-doped samples are composed of cubeoctaedric grains while for ND sample the microstructure is porous and vermicular. For clarity, only final microstructures after the standard sintering treatment are presented. Nevertheless, it must be noted that after heating at 1 °C min^{-1} up to 1450 °C, final microstructures seem to appear finer as Ti doping level increases (grain size of 2.1 and 1.4 μm for 16Ti and 96Ti, respectively) (Fig. 4).

The final grain size increases as the doping level increases up to 32Ti, whereas it decreases for higher Ti contents. The grain size distribution becomes more uniform for the highest Ti contents (64Ti and 96Ti).

Precipitates are observed in dense samples; they correspond to the Al_2TiO_5 phase. In the 64Ti-doped dense samples with grain sizes close to 1 μm, the largest precipitates are very similar to α-alumina grains, so their identification could only be easily performed by microanalysis. Precipitates are also located at triple junctions (Fig. 5a); they display extinction fringes also observed in neighboring grains implying elastic deformation of both phases. These strain contrasts result from the large expansion anisotropy of Al_2TiO_5. These precipitates have probably been formed at a later stage of the sintering process. Some small precipitates with geometrical shapes are also present along the GBs (Fig. 5b).

3.2.2. Microstructures at intermediate stages of sintering

The predominant modification of the microstructure in the presence of titanium is a lengthening of the elementary bricks that compose the porous single crystal colonies (Fig. 6a and b). Indeed this lengthening does not occur for other doping elements, as emphasized for a Y-doped sample in Fig. 6c. It is observed in all the Ti-doped alumina microstructures. For example, the microstructures of the 64Ti-doped samples, observed at various intermediate stages of sintering display only a change in brick size while the brick aspect ratio is the same, i.e. the morphology of the bricks is similar. The lengthening direction corresponds to a $\langle 1\,1\,\bar{2}\,0\rangle$ direction. For given titanium content, the heating rate does not influence the size of the elementary bricks.

An interesting microstructure is observed at the beginning of the densification and is emphasized in the 64Ti sample (1 °C min^{-1} to 1190 °C). The colonies contain some dense regions situated at triple junctions with other colonies (Fig. 7).

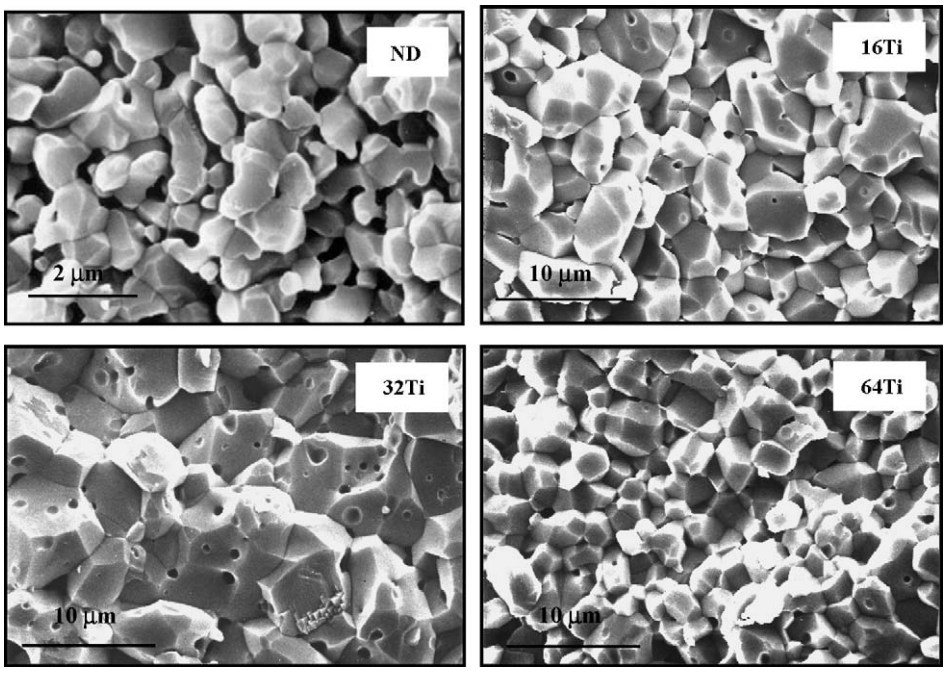

Fig. 4. Microstructures (SEM) of Ti-doped aluminas at the end of the standard sintering treatment (20 °C min^{-1} from 800 °C → 1450 °C + 4 h 15 min at 1450 °C). ND, undoped ($\rho = 3.05$ g cm^{-3}); 16Ti ($\rho = 3.83$ g cm^{-3}); 32Ti ($\rho = 3.91$ g cm^{-3}); 64Ti ($\rho = 3.91$ g cm^{-3}). Dense samples are composed of cubeoctaedric grains. The grain size increases as Ti level increases up to 3200 ppm, and then it decreases for higher levels.

In these regions the porosity inside the colonies is rapidly reduced. The density of these samples is about 50% of the theoretical density of α-alumina.

Some phenomena associated with the additional densification rate peak appear specifically on 16Ti- and 64Ti-doped samples:

(i) The presence of Al_2TiO_5 precipitates is effectively detected by X-ray diffraction after the AP densification rate peak for temperatures higher than 1190 °C. In the 16Ti sample, for standard sintering treatment interrupted after 5 min at soaking time at 1450 °C (20 °C min^{-1} → 1450 °C + 5 min) small precipitates (less than 100 nm diameter) are observed at triple junctions within dense regions. Dense regions are rarely observed in this still porous microstructure (Fig. 8).

(ii) Bricks of α-alumina contain 2-dimensionnal defects, more often parallel to a $\{1\,1\,\bar{2}\,0\}$ plane and thus perpendicular to the lengthening direction of grains. These defects sometimes appear faceted with facets parallel to other prismatic $\{1\,1\,\bar{2}\,0\}$ planes (Fig. 9). They occur both before and after the AP peak. They may be attached to a pore in the larger grain size samples.

(iii) Pseudo-periodic arrays of dislocations occur in numerous colonies in the 16Ti sample at the additional densification rate peak temperature (Fig. 10).

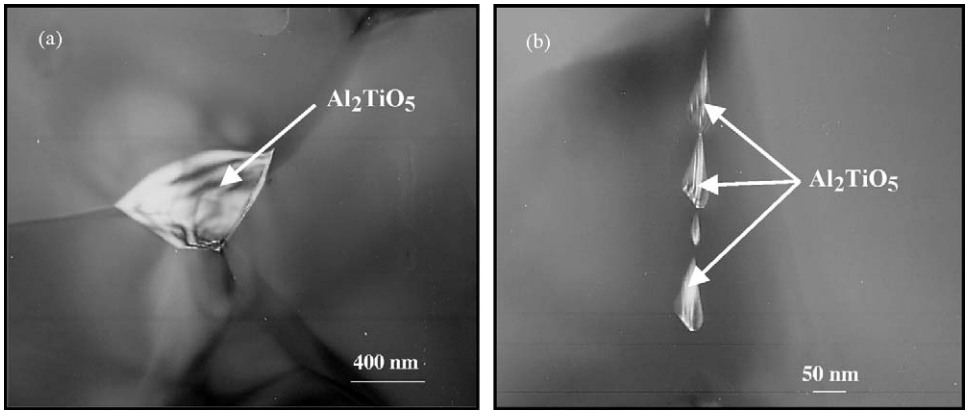

Fig. 5. TEM dark field images of Al_2TiO_5 precipitates (64Ti, 20 °C min^{-1} from 800 °C → 1450 °C + 4 h 15 min at 1450 °C, $\rho = 3.91$ g cm^{-3}). (a) At triple junctions, they present evidence of strain contrast. (b) Small precipitates are faceted at GBs.

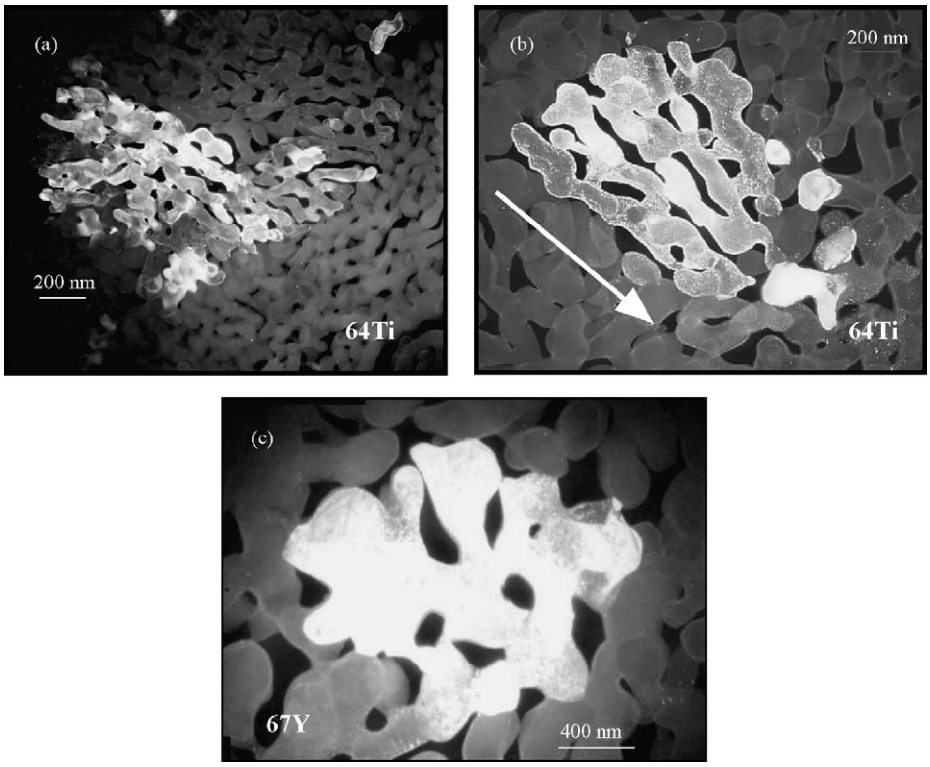

Fig. 6. Transmission Electron Microscopy (TEM) dark field images of 64Ti and 67Y doped samples at various intermediate stages of sintering, respectively (a) 64Ti, 1 °C min^{-1} → 1125 °C, $\rho = 1.75\,\mathrm{g\,cm^{-3}}$; (b) 64Ti, 1 °C min^{-1} → 1190 °C, $\rho = 1.83\,\mathrm{g\,cm^{-3}}$; and (c) 67Y, 1 °C min^{-1} → 1400 °C, $\rho = 1.97\,\mathrm{g\,cm^{-3}}$. The bricks inside the colonies appear elongated along the $\langle 1\,1\,\bar{2}\,0\rangle$ direction for Ti-doped samples.

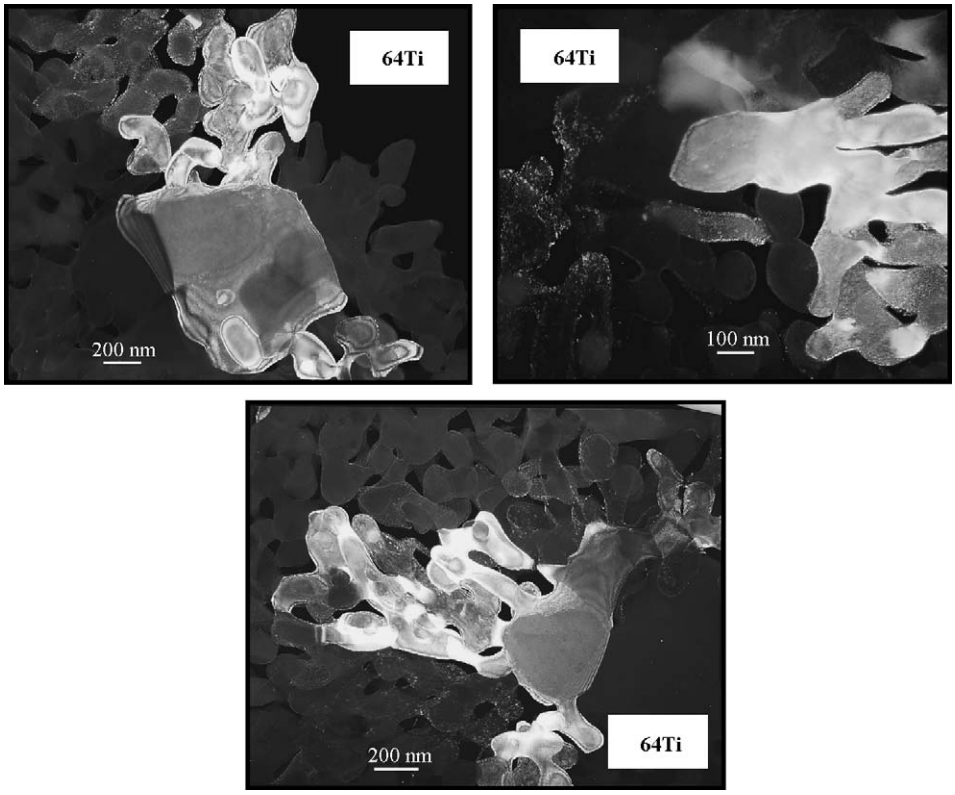

Fig. 7. TEM dark field images that emphasizes the beginning of densification in a 64Ti sample (1 °C/min from 800 °C up to 1190 °C). The densification occurs at the triple junctions between the colonies.

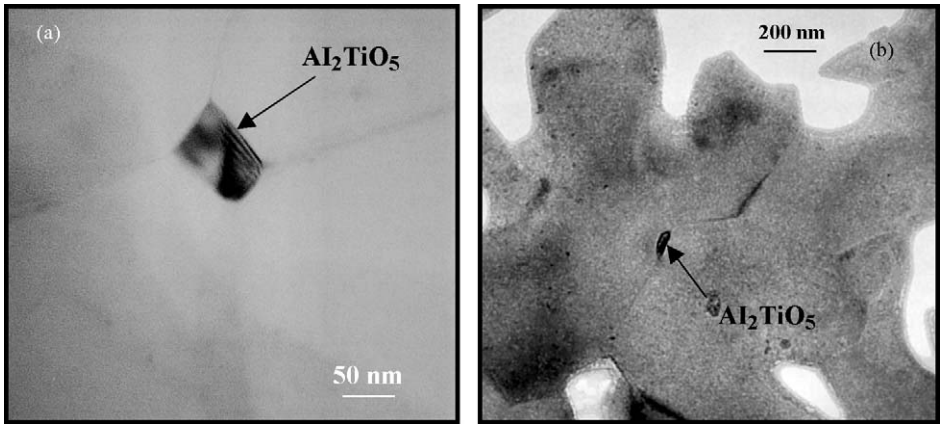

Fig. 8. TEM bright field micrograph of 16Ti sample (20 °C min^{-1} from 800 °C → 1450 °C + 5 min at 1450 °C). Small Al_2TiO_5 precipitates (<100 nm) occur in the dense regions of the sample.

(iv) Finally, numerous grain boundaries contain dislocation arrays or isolated dislocations. First investigations on the crystallographic parameters of 10 GBs containing dislocations show that these GBs may be near coincidence as well as general GBs.[43] It has been shown that dislocations can be stabilized by segregated species in general GBs.[44]

A TEM-EELS study has been carried out on the same materials.[45] It shows that all GBs contain titanium, and that the segregation width is narrow, less than 2 nm, whatever the density of the sample. This could result from a rapid diffusion of titanium ions towards and along the GBs.

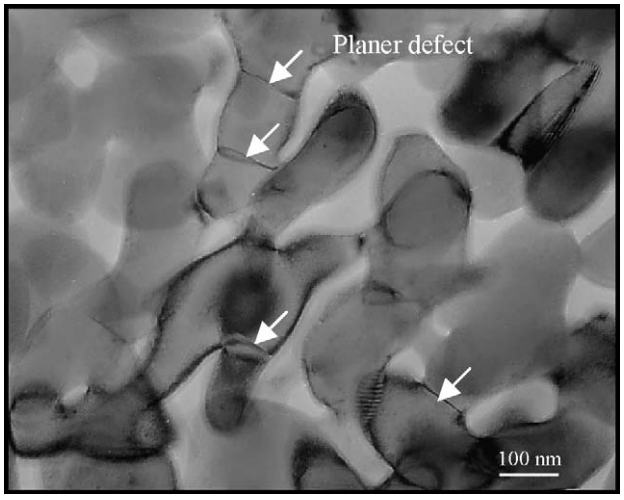

Fig. 9. TEM micrograph of planar defects (arrowed) inside the grains of 64Ti sample just after additional densification rate peak (1 °C min^{-1} → 1190 °C). The final temperature of the test corresponds roughly to the temperature for which the transient increase in densification (AP) takes place. The defects may be numerous inside a colony. They are always parallel to a prism plane $\{1\,1\,\bar{2}\,0\}$ and may be curved. Some intragranular pores occur in the nearly dense 16Ti sample.

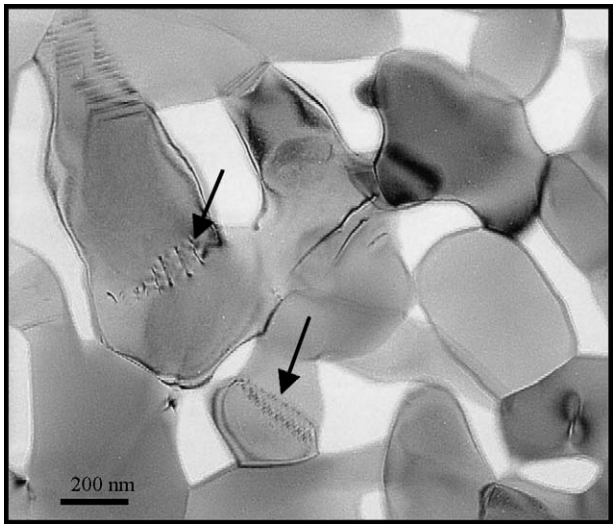

Fig. 10. TEM bright field image of the 16Ti sample (20 °C min^{-1} → 1450 °C + 5 min at 1450 °C) showing dislocation arrays inside the colonies ($\rho = 3.10$ g cm^{-3}).

4. Discussion

Effects of a doping element on a material are often described in terms of relationship between the properties affected and the overall doping concentration. In α-alumina, the solubility of most doping elements is rather small. Furthermore, the doping element may be distributed in different manners: in solid solution, segregated to GBs, and precipitated after saturation of both GBs and lattice. In such cases, it is important to identify the form of the dopant that has a dominant influence on the sintering mechanism. In the light of these considerations, we first discuss the influence of doping element on the γ → α phase transformation and then on the α-phase densification in relation with the spatial distribution of the doping element.

4.1. Influence of Ti-doping on γ–α phase transformation

The γ → α phase transformation is reported to be a type of nucleation and growth transformation. This transformation involves several processes, such as the nucleation of the α-phase, the rearrangement of γ-crystallites at α-alumina seeds or brick (grain) surfaces and the coalescence of bricks so as to form porous colonies of α-alumina grains with similar orientations.[13] All these processes may modify the temperature of the densification rate peak associated with the phase transformation. Generally speaking, one can say that doping elements seem to have no influence on the nucleation stage as inferred from the same phase transformation *starting temperature* (beginning of the increase in densification rate) whatever the dopant and dopant level (for a given heating rate). In this case, the nucleation site density should be the same in undoped and doped alumina. This suggests that in doped samples, whatever the doping level, the size of colonies should range from 1 to 2 μm in width. This is coherent with our observations on Ti-doped samples (Fig. 6).

However, the *temperature of the maximum* of the densification rate peak R1 varies with the doping species, which may influence the rearrangement of ions during the transformation: the oxygen ion lattice changes from a cubic face-centered packing to a nearly hexagonal packing. This transformation implies a redistribution of aluminum cations in octahedral sites involving their short-range diffusion in the transformation interface. If the doping element remains in solid solution in the growing α-phase during the transformation it would not influence the temperature of the maximum of the densification rate peak R1. For doping concentrations larger than their solubility in α-alumina, the doping ions are swept up by the transformation front and rejected to the closest surfaces and GBs.[46] The dopant segregation at surfaces of grains (bricks) should decrease the displacement rate of the front of transformation thus reducing the growth kinetic of α-phase and this would delay the maximum of the R1 peak temperature. This temperature increases slightly with titanium (for Ti/Al ≥ 1600 ppm) addition. It increases much more (50 °C) with zirconium and yttrium doping which have a low solubility in α-alumina (<15 ppm). An evoked explanation for this behavior, based on the role of the ionic radius, can be ruled out[47,48] as the ionic radii of magnesium and zirconium are similar.[49]

Finally, the *relative density variation* $\Delta\rho_R$ during the phase transformation is slightly reduced with Ti-doping; the higher the doping level, the smaller $\Delta\rho_R$. This could result from the lengthening of the bricks, which in turn does not favor the particle rearrangement and hence hinders densification.

4.2. Influence of Ti-doping on α-phase densification

Microstructures obtained at different stages of sintering reveal that Ti favors an *anisotropic growth of elementary bricks* along the $\langle 1\,1\,\bar{2}\,0\rangle$ direction, immediately after the γ → α phase transformation. This lengthening is more pronounced with increasing Ti content and duration of thermal treatment at 1450 °C. This anisotropy could be related to anisotropy of segregation.[34] Introduction of titanium leads to anisotropic surface energies[34] as is deduced from the morphology of internal pores in Ti-doped samples in comparison with undoped samples. In particular, the $\{1\,1\,\bar{2}\,0\}$ plane is not a low energy plane as it does not appear as a pore facet with Ti doping. This could explain why the $\langle 1\,1\,\bar{2}\,0\rangle$ direction is preferred as lengthening direction; anisotropic shapes of pores are observed in most orientations in relation with a higher energy of the prismatic plane $\{1\,1\,\bar{2}\,0\}$.[50] Anyway, the anisotropy has not been proved to occur at the γ → α phase transformation temperature.

Thus, the *rapid densification of colonies* in Ti-doped alumina could be attributed to the formation of a stacking of elongated elementary bricks inside a colony, which is more compact than the vermicular microstructure of undoped samples and so enhances the suppression of the intra-colony porosity (Fig. 11a and b). By such stacking mechanism the porous single-crystalline colonies rapidly transform into faceted fully dense α-grains.

After this stage of "internal" densification, a classical sintering process of dense cuboctaedric α-grains occurs. The R2 densification rate peak is equivalent to the main densification rate peak of α-alumina compacts sintered in constant heating rate conditions.[51] It corresponds to classical intermediate stage of sintering before the closure of porosity. Its temperature depends mainly on the average grain size: smaller is the grain size, lower is the temperature of R2 peak. For a 1 °C/min heating rate of α-alumina compacts, main densification rate peak temperatures of 1300, 1340 and 1380 °C, respectively correspond to 0.16, 0.4 and 1 μm grain

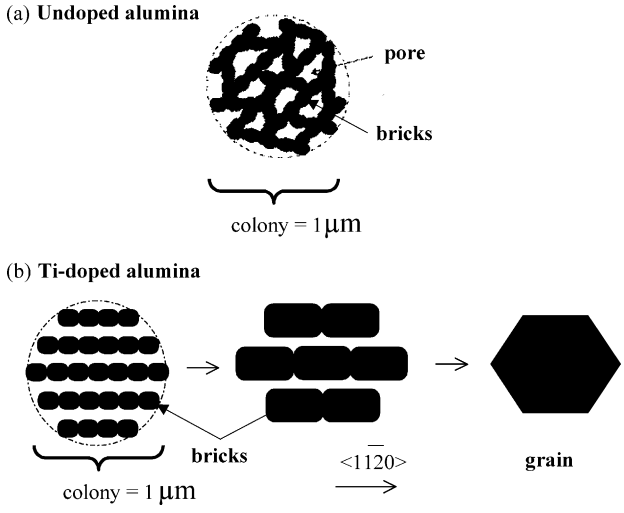

Fig. 11. Schematic illustration of (a) the colony microstructure in undoped alumina and (b) the mechanism of colony densification in Ti-doped alumina: the stacking of elongated bricks transforms the single crystalline porous colony into a dense faceted grain; in comparison the vermicular microstructure of undoped colonies (a) delays to much higher temperature the elimination of the intracolony porosity.

sizes.[51,52] So in the present study at 1400 °C, R2 peak temperature (Fig. 2) could correspond to dense colony or grain sizes slightly larger than 1 μm. This size is in fairly good agreement with colony or grain sizes observed in titanium doped samples at the corresponding temperature. The corresponding second densification rate peak R2 occurs at the same temperature in undoped and Ti-doped material, whatever the doping level may be (Fig. 3). This is expected since porous colonies and dense grains have the same size in both materials. This explains the beneficial influence of a high heating rate on densification: for experiments with a 20 °C min^{-1} heating rate, the nucleation site density should be higher, and hence the size of colonies (α-grains) should be smaller than for samples sintered with 1 °C/min leading to a better densification. Subsequently, only grain growth should take place and the density of material changes very little. These explanations are consistent with the sintering behaviors observed here for both 1 °C min^{-1} and 20 °C min^{-1} heating rate.

As in yttrium-doped alumina,[9] an *additional densification rate* peak is observed during sintering. This transient increase in densification rate is associated with a transition between a microstructure with only intergranular segregation and a microstructure for which precipitation of $Y_3Al_5O_{12}$ occurs at triple junctions. As grain size increases, the total area of interfaces decreases and the dopant concentration at GBs increases until saturation of dopant at GBs and ensuing precipitation. During this transition, the increase in densification rate is attributed, in the case of yttrium, to an increase in intergranular diffusivity resulting from an yttrium supersaturation at GBs leading to precipitation.[24,53–55] Similar mechanisms with precipitation of $Al_2T_iO_5$ can be invoked for Ti-doped alumina. The temperature of this additional densification rate peak is higher for lower doping levels. The transition depends only on grain size and thus occurs at higher temperatures, i.e. at higher grain sizes. Also the intensity of the corresponding peak is higher as it occurs for a well-dense microstructure. This observation is in agreement with an enhancement of intergranular or surface/interface diffusion that results from a supersaturation of dopants at GBs or at brick surfaces and interfaces before precipitation: the supersaturation should be much more pronounced if GBs and interfaces are well-defined between and inside dense colonies, respectively.

It is worth noting that this transient increase in densification rate promotes concurrent grain growth. In fact, for the final microstructures for standard sintering treatment, the grain size of 32Ti sample is larger than that of highly doped materials (64Ti and 96Ti). This 32Ti sample presents simultaneous α-phase densification (R2) and a "segregation–precipitation" transition (AP). For higher doping levels, grain boundary or interface saturation occurs at lower temperatures and for lower densities. Consequently, Al_2TiO_5 precipitates at GBs or interfaces limit grain growth, once the densification is achieved. Similar considerations could explain why the 16Ti sample exhibits larger grain size after sintering at 1 °C min^{-1} up to 1450 °C.

This transient increase in densification rate is associated with the formation of stacking faults and dislocation arrays inside the grains.[45] These defects may result from the creation of numerous point defects that originate from a rapid diffusion of species necessary to supply the precipitates during the transition. As Ti, Al and O have different diffusion coefficients local excess in point defects may occur. This is in agreement with the presence of dislocations that behave as sources and sinks for defects. Similar behavior has been observed in another ceramic, Ca-doped TiO_2.[56] At first stages of precipitation of $CaTiO_3$, small grains contain numerous planar defects attributed to an "understoichiometry" in oxygen ions. However, a relationship with precipitation is evoked without interpretation.[56]

Results on the evolution of precipitation with grain size make it possible to establish a *microstructural map* showing the "segregation–precipitation" transition (Fig. 12); the results obtained by other authors on dense materials are also included.[37,57–60] As already shown for Y-doped alumina,[9] there is a gap separating the region for which the doping element is segregated at GBs (open symbols) from the region where the dopant is both segregated and precipitated (full symbols). In this gap, it is possible to draw a straight line with a slope of −1, which indicates that the transition grain size should vary as the inverse of the cationic ratio.[28] In the present case, porous samples present surface segregation as

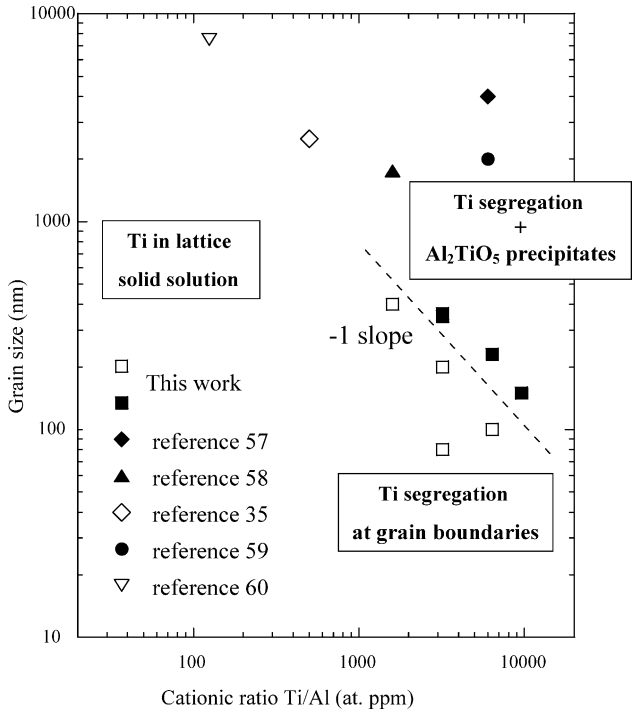

Fig. 12. Microstructural map for Ti-doped alumina showing the transition "segregation–precipitation" (for open symbols no second phase is detected, for filled symbols Al_2TiO_5 precipitates have been observed). This map allows to show the different states under which a doping element may be distributed: as a lattice solid solute, as a grain boundary segregated element beyond saturation of the lattice solid solution, and engaged in a second phase precipitate upon saturation of both GBs and lattice solid solution.

well as intergranular segregation. The precipitation could occur for a slightly larger grain size. In any case, differences on grain size estimation cannot be readily detected on a logarithmic scale (Fig. 12). This map leads to the prediction of the presence or not of precipitation from the knowledge of the overall dopant content and grain size. The solubility limit inside grains appears to be close to 500 ppm. This value is in good agreement with previous determination.[61]. In Ref.[14], the authors reported a change in mechanism from grain boundary to volume diffusion that was a function of particle size and titanium content. The transition particle radius was between 0.5 and 1 μm. Such transition or change could correspond to the transition between GB segregation and precipitation.

The microstructural transition may play a role in the onset of the development of anisotropic grain growth that has been shown to occur in a narrow range of TiO_2 concentrations for a given grain size. Grain growth experiments[41] in alumina doped with 960 ppm Ti/Al display anisotropic grains once the grain size reaches about 1 μm (initial grain size = 400 nm). According to our results, this grain size corresponds to the transition between segregation and precipitation for this titanium level (see Fig. 12). Interestingly, no anisotropic grain growth is observed for a higher doping level (≅4000 ppm).

In that case, the transition does not occur as the initial grain size is larger than the grain size for which the transition should occur. During the transition, saturated GBs may display higher migration rates than the other GBs as already suggested for yttrium doping.[24] Strong variations in GB chemistry from one GB to another one must occur as all GBs are not saturated with dopant at the same moment, with probably site competition effect between Ti and other major impurities, such as silicon or calcium. This is in agreement with the fact that anisotropic grain growth occurs when a small population of grains has reached a critical size in the microstructure.[41]

5. Conclusion

The $\gamma \rightarrow \alpha$ phase transformation involves two main processes: nucleation of α-phase and growth of more or less porous colonies consisting of elementary bricks with similar crystallographic orientation. Doping elements seem to have no influence on the number of nucleation sites as inferred from the similar temperatures of the beginning of the phase transformation whatever the doping nature and level. Titanium strongly enhances the densification regime (R2) in α-phase by an anisotropic growth or coalescence of the elementary bricks inside porous colonies. The formation of compact stacking of elongated elementary bricks favors the rapid elimination of intra-colony porosity and so allows the classical sintering of dense grains of α-phase. Additional densification rate peaks are clearly observed for titanium and yttrium doped materials: the higher the doping level, the lower the temperature of these additional peaks. They correspond to a microstructural transition from doping element segregation at grain boundaries or at surfaces and interfaces to precipitation of a second phase rich in doping species. These additional densification rate peaks are explained by an enhancement of the intergranular or surface/interface diffusion that results from a supersaturation of dopants at GBs or at brick surfaces and interfaces before precipitation: the supersaturation is much more pronounced if GBs and interfaces are well-defined, respectively between and inside dense colonies. Such microstructural transitions, i.e. precipitation grain size for a given doping ratio, can be predicted from segregation–precipitation maps.

Acknowledgements

The authors wish to thank Baikowski Chimie for providing high-purity γ-alumina raw powders. We are also pleased to thank Dr. D. Bouchet and Dr. P. Bowen for valuable discussions and undergraduate students (M. Chapoy and M. Niox) for their experimental contributions. Professor J.P. Chevalier is acknowledged for his critical reading of the manuscript.

References

1. Ding, X. Z. and Liu, X. H., Correlation between anatase to rutile transformation and grain growth in nanocrystalline titania powders. *J. Mater. Res.*, 1998, **13**, 2556–2559.
2. Liao, S. C., Pae, K. D. and Mayo, W. E., High pressure and low temperature sintering of bulk nanocrystalline TiO_2. *Mater. Sci. Eng.*, 1995, **A204**, 152–1s59.
3. Chen, I. W. and Wang, X. H., Sintering dense nanocrystalline ceramics without final-stage grain growth. *Nature*, 2000, **404**, 168–171.
4. Dynys, F. W. and Halloran, J. W., Alpha alumina formation in alum-derived γ-alumina. *J. Am. Ceram. Soc.*, 1982, **65**, 442–448.
5. Messing, G. L. and Kumagai, M., Low-Temperature sintering of α-alumina seeded boehmite gels. *Am. Ceram. Soc. Bull.*, 1994, **73**, 88–91.
6. Legros, C., Carry, C., Bowen, P. and Hofmann, H., Sintering of a transition alumina: effects of phase transformation, powder characteristics and thermal cycle. *J. Eur. Ceram. Soc.*, 1999, **19**, 1967–1978.
7. Mishra, R. S., Lesher, C. E. and Mukherjee, A. K., High pressure sintering of nanocrystalline gamma-Al_2O_3. *J. Am. Ceram. Soc.*, 1996, **79**, 2989–2992.
8. Xue, L. A. and Chen, I. W., Influence of additives on the gamma to alpha transformation of alumina. *J. Mat. Sci. Lett.*, 1992, **1**, 443–445.
9. Carry, C., Bowen, P., Herbst, F. and Legros, C., The effect of yttrium and zirconium on sintering of a transition alumina. In *Sintering Science and Technology*, ed. R. M. German, G. L. Messing and R. G. Cornwall. The Pennsylvania State University, State College PA, USA, 2000, pp. 177–182.
10. Bowen, P., Charvin, O., Hofmann, H., Carry, C. and Herard, C., Processing of nanosized powders, a bimodal slip casting approach. *Ceram. Process. Sci.*, pp. 211–218. In *Ceram. Trans.*, *Vol* 83, ed. G.L. Messing, F.F. Lange and S. Hirano. American Ceramic Society, 1998.
11. Bowen, P., Staiger, M., Hofmann, H. and Carry, C., Processing effects on the sintering behavior of transition alumina powders. In *Sintering Science and Technologies*, ed. R. M. German, G. L. Messing and R. G. Cornwall. The Pennsylvania State University, State College PA, USA, 2000, pp. 171–176.
12. Godlinski, D., Kuntz, M. and Grathwohl, G., Transparent alumina with submicrometer grains by float packing and sintering. *J. Am. Ceram. Soc.*, 2002, **85**(10), 2449–2456.

13. Legros, C., Herbst, F., Lartigue-Korinek, S., Carry, C. and Bowen, P., Frittage d'alumines nanostructurées: rôle de différents paramètres. *Rev. Met. Paris*, 2002, **12**, 1073–1080.
14. Bagley, R., Cutler, I. B. and Johnson, D. L., Effect of TiO_2 on initial sintering of Al_2O_3. *J. Am. Ceram. Soc.*, 1970, **53**, 136–141.
15. Cutler, I. B., Bradshaw, C., Christenson, C. and Hyatt, E., Sintering of alumina at temperatures of 1400 °C and below. *J. Am. Ceram. Soc.*, 1957, **40**, 134–139.
16. Cahoon, H. and Christenson', C., Sintering and grain growth of alpha-alumina. *J. Am. Ceram. Soc.*, 1956, **39**, 337–344.
17. Hamano, K., Hwang, C., Nagagawa, Z. and Ohya, Y., Effects of TiO_2 on sintering of alumina ceramics. *Yogyo Kyokai Shi*, 1986, **94**(5), 505–511.
18. Song, H. and Coble, R., Origin of growth kinetics of platelike abnormal in liquid–phase-sintered alumina. *J. Am. Ceram. Soc.*, 1990, **73**, 2077–2085.
19. Song, H. and Coble, R., Morphology of platelike abnormal in liquid-phase-sintered alumina. *J. Am. Ceram. Soc.*, 1990, **73**, 2086–2090.
20. Kim, Y. M., Song, S. H. and Kim, D. Y., Anisotropic abnormal grain growth in TiO_2/SiO_2-doped alumina. *J. Am. Ceram. Soc.*, 2000, **83**, 2809–2812.
21. Li, C.W. and Kingery, W.D., Solute segregation at grain boundaries in polycrystalline Al_2O_3. In *Advances in Ceramics, Structure and properties of MgO and Al_2O_3Ceramics*, *Vol* 10, ed. W.C. Kingery. ACS, Columbus Ohio, 1984, pp. 367–378.
22. Swiatnicki, W., Lartigue-Korinek, S. and Laval, J. Y., Grain boundary structure and intergranular segregation in Al_2O_3. *Acta Metall. Mater.*, 1995, **43**, 795–805.
23. Gavrilov, K. L., Bennison, S. J., Mikeska, K. R., Chabala, J. M. and Levi-Setti, R., Silica and magnesia dopant distributions in alumina by high-resolution scanning secondary ion mass spectrometry. *J. Am. Ceram. Soc.*, 1999, **82**, 1001–1008.
24. Lartigue-Korinek, S., Carry, C. and Priester, L., Multiscale aspects of the influence of yttrium on microstructure, sintering and creep of alumina. *J. Eur. Ceram. Soc.*, 2002, **22**, 1525–1541.
25. Ragan, D. D., Mates, T. and Clarke, D. R., Effect of yttrium and erbium ions on epitaxial phase transformations in alumina. *J. Am. Ceram. Soc.*, 2003, **86**(4), 541–545.
26. Gutierrez-Alejandre, A., Gonzalez-Cruz, M., Trombetta, M., Busca, G. and Ramirez, J., Characterization of alumina-titania mixed oxide supports. Part II: Al_2O_3-based supports. *Microporous Mesoporous Mater.*, 1998, **23**, 265–275.
27. Legros, C., Herbst, F. and Carry, C., Influence of magnesia on sintering of transition alumina. In *Ceramics-Processing, Reliability, Tribology and Wear, EUROMAT 99*, *12*, ed. G. Müller. DGM and WILEY-VCH, 2000, pp. 23–28.
28. Gruffel, P. and Carry, C., Effect of grain size on yttrium grain boundary segregation in fine grained alumina. *J. Eur. Ceram. Soc.*, 1993, **11**, 189–199.
29. Prot, D., Le Gall, M., Huntz, A. M., Lesage, B. and Monty, C., Self-diffusion in α-Al_2O_3, IV. Oxygen grain-boundary self-diffusion in undoped and yttria doped alumina polycrystals. *Phil. Mag. A*, 1996, **73**, 935–949.
30. Yoshida, H., Okada, K., Ikuhara, Y. and Sakuma, T., Improvement of high temperature creep resistance in fine-grained Al_2O_3 by Zr^+ segregation in grain boundaries. *Phil. Mag. Lett.*, 1997, **76**, 9–14.
31. Yoshida, H., Yamamoto, T., Ikuhara, Y. and Sakuma, T., A change in the chemical bonding strength and high temperature creep resistance in alumina with lanthanid oxide doping. *Phil. Mag. A*, 2002, **82**, 511–525.
32. Lartigue, S., Priester, L., Dupau, F., Gruffel, P. and Carry, C., Dislocation activity and differences between tensile and compressive creep of yttria doped alumina. *Mat. Sci. Eng.*, 1993, **A164**, 211–215.
33. Yoshida, H., Ikuhara, Y. and Sakuma, T., Grain boundary electronic structure related to the high temperature creep resistance in polycrystalline α-Al_2O_3. *Acta Mater.*, 2002, **50**(11), 2955–2966.
34. Kitayama, M. and Powers, J. D., Microdesigned interfaces: new opportunities for studies of surfaces and grain boundaries. In *Ceramic microstructure:control at the atomic level*, ed. A. P. Tomsia and A. M. Glaeser. Plenum Press, New York, 1998, pp. 229–238.
35. Powers, J. D. and Glaeser, A. M., Titanium effects on sintering and grain boundary mobility of alumina. *Ceram. Eng. Sci. Proc.*, 1997, **18**(4), 617–623.
36. Brook, R. J., Effect of TiO_2 on the initial sintering of Al_2O_3. *J. Am. Ceram. Soc.*, 1972, **55**, 114–115.
37. Kebbede, A., Parai, J. and Carim, A. H., Anisotropic Grain Growth in α-Al_2O_3 with SiO_2 and TiO_2 Additions. *J. Am. Ceram. Soc.*, 2000, **83**(11), 2845–2851.
38. Handwerker, C. A., Morris, P. A. and Coble, R. L., Effects of chemical inhomogeneities on grain growth and microstructure in Al_2O_3. *J. Am. Ceram. Soc.*, 1989, **72**, 130–136.
39. Bennison, S. and Harmer, M. P., Swelling of hot-pressed Al_2O_3. *J. Am. Ceram. Soc.*, 1985, **68**(11), 591–597.
40. Morgan, P. E. D. and Koutsoutis, M. S., Phase studies concerning sintering in alumina doped with Ti^+. *J. Am. Ceram. Soc.*, 1985, **68**(6), C156–C158.
41. Horn, D. S. and Messing, G. L., Anisotropic grain growth in TiO_2-doped alumina. *Mat. Sci. Eng.*, 1995, **A195**, 169–178.
42. Vereshchagin, V. I., Zelinskii, V. Yu., Khabas, T. A. and Kolova, N. N., Kinetics and mechanism of conversion of low-temperature forms of alumina into α-Al_2O_3 in presence of additives. *Zh. Prikl. Khim.*, 1982, **55**, 1946–1951.
43. Grimmer, H., Bonnet, R., Lartigue, S. and Priester, L., Theoretical and experimental descriptions of grain boundaries in rhombohedral alpha-Al_2O_3. *Phil. Mag. A*, 1990, **61**, 493–509.
44. Lartigue-Korinek, S. and Dupau, F., Grain boundary behavior in superplastic Mg-doped alumina with yttria codoping. *Acta Metall. Mater.*, 1994, **42**, 293–302.
45. Bouchet, D., Herbst, F., Lartigue-Korinek, S. and Colliex, C., Titanium segregation behavior during sintering of α-Al_2O_3: a TEM-EELS study. *Proceedings of the International Conference on Microscopy and Microanalysis*, Durban, SA, September 2002, pp. 537–539.
46. Clarke, D. R., Epitaxial phase transformations in aluminium oxide. *Phys. Stat. Sol. A*, 1998, **166**, 183–196.
47. Okada, K., Hattori, A., Taniguchi, T., Nukui, A. and Das, R. N., Effect of divalent cation additives on the gamma to alpha alumina phase transition. *J. Am. Ceram. Soc.*, 2000, **83**, 928–932.
48. Okada, K., Hattori, A., Kamesshima, Y., Yasumori, A. and Das, R. N., Effect of monovalent cation additives on the gamma to alpha alumina phase transition. *J. Am. Ceram. Soc.*, 2000, **83**, 1233–1236.
49. Shannon, R. D., Revised effective ionic radii and systematic studies of interatomic distances in halides and chalcogenides. *Acta Cryst.*, 1976, **A32**, 751–767.
50. Choi, J. H., Kim, D. Y., Hockey, B. J., Wiederhorn, S. M., Handwerker, C. A., Blendell, J. E. *et al.*, Equilibrium shape of internal cavities in sapphire. *J. Am. Ceram. Soc.*, 1997, **80**, 62–68.
51. Sato, E. and Carry, C., Effect of powder granulometry and pretreatment on sintering behavior of submicron-grained α-alumina. *J. Eur. Ceram. Soc.*, 1995, **15**, 9–16.
52. Sato, E. and Carry, C., Yttria doping and sintering of submicron-grained α-alumina. *J. Am. Ceram. Soc.*, 1996, **79**(8), 2156–2160.
53. Gülgün, M. A., Putlayev, V. and Rühle, M., Effects of yttrium doping alpha-alumina. I. Microstructure and microchemistry. *J. Am. Ceram. Soc.*, 1999, **82**(7), 1849–1856.
54. Gülgün, M.A. and Rühle, M., Yttrium in polycrystalline α-alumina, *Key Eng. Mat.*, *Vols* 171–174, pp. 793–800, Edited by Trans Tech Publications, Switzerland, 2000.
55. Wang, C. M., Cargill, G. S., Chan, H. M. and Harmer, M. P., Structural features of Y-saturated grain boundaries in alumina. *Acta Mater.*, 2000, **48**, 2579–2591.
56. Terwilliger, C. D. and Chiang, Y. M., Size dependent solute segregation and total solubility in ultrafine polycrystals: Ca in TiO_2. *Acta Metall. Mater.*, 1995, **43**, 319–328.

57. Erkalfa, H., Misirli, Z. and Baykara, T., The effect of TiO_2 and MnO_2 on densification and microstructural development of alumina. *Ceram. Int.*, 1998, **24**, 81–90.
58. Langensiepen, R. A., Tressler, R. E. and Howell, P. R., A preliminary study of precipitation in Ti^{+}-doped alumina. *J. Mat. Sci.*, 1983, **18**, 2771–2776.
59. Shimura, S. and Bowen, H.K., Effects of foreign oxides on grain growth and densification of sintered Al_2O_3. *Ceramic Transactions. Ceramic Powder Science* II, *Vol* 1, 1991, pp. 840–847.
60. Harmer, M., Roberts, E. W. and Brooks, R. J., Rapid sintering of pure and doped alpha Al_2O_3. *Trans. Br. Ceram. Soc.*, 1979, **78**(1), 22–25.
61. Mohapatra, S. K. and Kröger, F. A., Defect structure of alpha Al_2O_3 doped with titanium. *J. Am. Ceram. Soc.*, 1977, **60**, 381–387.